Available online at www.sciencedirect.com
SCIENCE DIRECT®
Mechanical Systems and Signal Processing 18 (2004) 291–315
Mechanical Systems and Signal Processing
www.elsevier.com/locate/jnlabr/ymssp

Reducing the effect of truncation error in spatial and pointwise models of resonant systems with damping

Dunant Halim[a,*], S.O. Reza Moheimani[b]

[a] Department of Mechanical Engineering, The University of Adelaide, SA 5005, Australia
[b] School of Electrical Engineering and Computer Science, The University of Newcastle, NSW 2308 Australia

Received 10 May 2002; received in revised form 14 February 2003; accepted 26 February 2003

Abstract

This paper is concerned with finding analytical solutions to the problems of reducing the effect of truncation error in models of resonant systems that include damping. Pointwise and spatial models of resonant systems are both considered in the paper. It is known that the truncation of an infinite-dimensional model produces errors in the zero locations and zero-frequency content of the system. Our approach is to add a feedthrough term to the truncated model to reduce the uncertainty caused by neglected dynamics. This will improve the accuracy of the model by reducing the errors in the zero locations and zero-frequency content of the system, which is important in ensuring the closed-loop system's robustness when a feedback controller is implemented. The optimal feedthrough terms are determined by minimising the weighted $\mathscr{H}_2$ norm and spatial $\mathscr{H}_2$ norm of the error systems associated with the pointwise and spatial models, respectively. The existence of analytical solutions for optimal feedthrough terms allows models of resonant systems to be compensated in a straightforward manner. Simulation results are presented to demonstrate the effectiveness of our approach in reducing the effect of truncation error.

1. Introduction

A resonant system with spatially distributed nature consists of, theoretically, an infinite number of modes. Modal analysis method is commonly used to obtain a model of such a system [1,2]. It is known that high-frequency modes also contribute to the dynamics at low frequencies. Thus, a model may have to include a relatively high number of high-frequency modes to capture the low-frequency dynamics with acceptable accuracy. This yields a model with a relatively high order.

*Corresponding author. Tel.: +61-8-83036941; fax: +61-8-83034367.
E-mail addresses: dunanth@mecheng.adelaide.edu.au (D. Halim), reza@ee.newcastle.edu.au (S.O.R. Moheimani).

0888-3270/04/$ - see front matter
doi:10.1016/S0888-3270(03)00039-6

However, for control design purposes, it is often impractical to use a relatively high-order model since the controller's order will tend to be large as well. Although the controller's size can be reduced at a later stage, a further analysis is needed since the order reduction may adversely affect the closed-loop performance and stability. Furthermore, using a higher- order model may result in numerical difficulties.

A number of approaches for model reduction have been developed, such as model reduction via balanced realisation (see, for example [3,4]). However, since the approaches are generally based on the order reduction of a finite-dimensional model, there is a limit on how many out-of-bandwidth modes can be included when a resonant system with a spatially distributed nature is considered.

A simpler approach for model reduction is by direct truncation. Here, higher frequency modes, i.e. out-of-bandwidth modes, are ignored assuming that their collective impact on the in-bandwidth dynamics is minor. However, although the removal of the out-of-bandwidth modes does not affect the in-bandwidth poles of the system, it may perturb the in-bandwidth zeros [5–8]

One approach to minimising the truncation error is to add a feedthrough term to the truncated model to correct the locations of the in-bandwidth zeros. The technique is known in the aeroelasticity literature as the mode acceleration method [9] and has been recently re-visited in [5–8]. In the mode acceleration method, the feedthrough term consists of the sum of d.c., (zero-frequency) contents of all the truncated out-of-bandwidth modes [5,9]. However, this only reduces the d.c. error to zero. The error at higher frequencies, within the bandwidth of interest, could still be large. Furthermore, it is also not clear how the multivariable systems should be dealt with.

Another approach to minimising the truncation error is proposed in [7] by minimising the weighted $\mathscr{H}_2$ norm of the truncation error. In [7], however, it is assumed that there is no damping in the system, and then an analytical solution is presented for the optimal feedthrough terms for multivariable pointwise models.

Furthermore, when one deals with spatially distributed systems, often a spatial model of the system is required. It is also desirable to limit the size of the model for control design purposes. This leads to the need of compensating for the truncation error in the truncated spatial model. A technique is proposed in [6] for finding a feedthrough term that minimises the weighted spatial $\mathscr{H}_2$ norm of the truncation error. This technique is based on the idea of spatial $\mathscr{H}_2$ norm for spatially distributed systems introduced in [10,11], The main assumption made in [6] is that the system contains no damping.

The techniques proposed in [6,7] are useful in finding optimal feedthrough terms for models of resonant systems since the analytical solutions are available. However, all physical systems have some damping associated with them. Therefore, the no-damping assumption may only be acceptable if the damping is very small. When the system has reasonable damping, the effect of damping can be significant and can no longer be ignored. The feedthrough terms found by neglecting the damping effect may not be close to optimal anymore. It is possible, however, to use numerical approaches to find the correction terms for systems that include damping. For example, in [12], a convex optimisation via LMI is developed to calculate the optimal feedthrough terms for systems with damping. However, the number of out-of-bandwidth modes that can be included is computationally limited. This paper extends the method of [6,7] for the systems that include damping. The existence of the analytical solutions for the feedthrough terms allows the feedthrough terms to be readily calculated with no limitation on how many out-of-bandwidth

modes that can be included. Therefore, more accurate reduced order models can be achieved with the proposed solutions.

2. Models of resonant systems

Consider a typical multi-input multi-output (MIMO) model of a resonant system that is obtained from modal analysis:

$$G(s) = \sum_{i=1}^{\infty} \frac{F_i}{s^2 + 2\zeta_i \omega_i s + \omega_i^2}. \tag{1}$$

Here, ω_i is the resonance frequency of mode i and $F_i \in \mathbf{R}^{m\times n}$. Hence, $G(s)$ maps the inputs, $u \in \mathbf{R}^n$, to the outputs, $y \in \mathbf{R}^m$. This model represents the pointwise model of the system that relates n input signals to m output signals.

Notice that a proportional damping term has been added to each mode. This limits the vibrational energy at resonance. Although it is difficult to model the damping in structures accurately, the proportional damping is often sufficient to obtain a reasonable and practical model of the structure. The damping factor associated with each mode can later be determined by, performing modal tests on the structure [13].

Spatial model, multi-Input, infinite-output (MIIO), of a resonant system can be represented by

$$G_r(s, r) = \sum_{i=1}^{\infty} \frac{\phi_i(r) P_i}{s^2 + 2\zeta_i \omega_i s + \omega_i^2} \tag{2}$$

where $P_i \in \mathbf{R}^{1\times n}$ and the transfer function, $G_r(s, r)$, maps the input, $u(t) \in \mathbf{R}^n$ to the output, $y(t, r) \in \mathbf{R} \times \mathscr{R}$ where $r \in \mathscr{R}$. For example, $\mathscr{R} = [0, \mathrm{L}]$ for a beam with length L, and $\mathscr{R} = [0, \mathrm{a}] \times [0, \mathrm{b}]$ for a plate with size $a \times b$. For a beam under flexural vibration, the spatial output, y, might be the transverse displacement at point r along the beam. For a rod under torsional vibration, the spatial output might be the angular displacement at point r along the rod.

Also, Φ_i is the eigenfunction associated with mode i which satisfies the following orthogonality property:

$$\int_{\mathscr{R}} \phi_i(r)\phi_j(r)dr = \Phi_i^2 \delta_{ij} \tag{3}$$

where Φ_i and δ_{ij} are a constant and the Kronecker delta function, respectively.

In the modal analysis, the systems in Eqs. (1) and (2) consist of an infinite number of modes. One simple way to reduce the size of the model is by direct truncation. Suppose that only a particular bandwidth is of interest. Only N lowest frequency modes inside the bandwidth are included in the model. Hence, by direct truncation, the pointwise model can then be written as

$$G_N(s) = \sum_{i=1}^{N} \frac{F_i}{s^2 + 2\zeta_i \omega_i s + \omega_i^2} \tag{4}$$

and for the spatial model,

$$G_{rN}(s) = \sum_{i=1}^{N} \frac{\phi_i(r)P_i}{s^2 + 2\zeta_i\omega_i s + \omega_i^2} \tag{5}$$

Note that the higher frequency modes, i.e. out-of-bandwidth modes, are ignored assuming that their effects on the in-bandwidth frequencies are minor. However, this direct truncation perturbs the zero locations and the d.c. (zero-frequency) content of the truncated model [5–8]. Reduction of this truncation error would improve the accuracy of the model and, as a consequence, the robustness of the closed-loop system when a feedback controller is incorporated. The task of this paper is to develop an analytical solution for correcting the truncated model for which the truncation error can be compensated.

3. Problem statement for MIMO pointwise models

Consider the pointwise system whose truncated model is given in Eq. (4). The approach is based on finding a suitable feedthrough term, which is a constant matrix $K \in \mathbf{R}^{m\times n}$, to compensate for the truncation error resulting from the removal of modes $N+1$ to ∞. The corrected model, $\hat{G}(s)$, then can be written as

$$\hat{G}(s) = G_N(s) + K. \tag{6}$$

The matrix K is determined by finding the K that minimises the weighted error between the full-order model and the corrected model. The method used here follows [7], where the cost function is defined as

$$J = \|W(s)(G(s) - \hat{G}(s))\|_2^2 \tag{7}$$

with W a diagonal matrix whose diagonal elements are ideal low-pass filters,

$$W = \mathrm{diag}(w, w, \ldots, w) \tag{8}$$

and

$$w(\,jw) = \begin{cases} 1, & -w_c \leqslant w \leqslant w_c \\ 0, & \text{otherwise} \end{cases} \tag{9}$$

in which $\omega_c \in (\omega_N, \omega_{N+1})$ is the cut-off frequency of each filter that is placed between the highest in-bandwidth mode and the lowest out-of-bandwidth mode. Hence, one considers only the truncation error up to the cut-off frequency.

Let

$$\tilde{G}(s) = \sum_{i=N+1}^{\infty} \frac{F_i}{s^2 + 2\zeta_i\omega_i s + \omega_i^2} \tag{10}$$

so $G(s) = G_N(s) + \tilde{G}(s)$. Then the cost function J in Eq. (7) can be written as follows:

$$\begin{aligned} J &= \|W\tilde{G}\|_2^2 + \|WK\|_2^2 - \left(\langle W\tilde{G}, WK\rangle + \langle WK, W\tilde{G}\rangle\right) \\ &= \|W\tilde{G}\|_2^2 + \frac{1}{2\pi}\int_{-\infty}^{\infty} \operatorname{trace}\left\{K^T W(j\omega)^* W(j\omega)K\right\} \mathrm{d}\omega \\ &\quad - 2 \times \frac{1}{2\pi}\int_{-\infty}^{\infty} \operatorname{Re}\left\{\operatorname{trace}\left\{\tilde{G}(j\omega)^* W(j\omega) * W(j\omega)K\right\}\right\} \mathrm{d}\omega \\ &= \|W\tilde{G}\|_2^2 + \frac{1}{2\pi}\int_{-\omega_c}^{\omega_c} \operatorname{trace}\left\{K^T K\right\} \mathrm{d}\omega - 2 \times \frac{1}{2\pi}\int_{-\omega_c}^{\omega_c} \operatorname{Re}\left\{\operatorname{trace}\left\{\tilde{G}(j\omega) * K\right\}\right\} \mathrm{d}\omega \end{aligned} \tag{11}$$

where $\langle U, V\rangle = 1/(2\pi)\int_{-\infty}^{\infty} \operatorname{trace}\{U^*(j\omega)V(j\omega)\}\,\mathrm{d}\omega$.

Differentiating the cost function J with respect to K (see [14], p. 592) and setting this value to a zero vector for optimality

$$\frac{\mathrm{d}J}{\mathrm{d}K} = 2 \times 2\omega_c \times \frac{1}{2\pi}K_{\mathrm{opt}} - 2 \times \frac{1}{2\pi}\int_{-\omega_c}^{\omega_c} \operatorname{Re}\left\{\tilde{G}(j\omega)\right\} \mathrm{d}\omega = 0. \tag{12}$$

The optimum value of K is then found to be

$$K_{\mathrm{opt}} = \frac{1}{2\omega_c}\int_{-\omega_c}^{\omega_c} \operatorname{Re}\left\{\tilde{G}(j\omega)\right\} \mathrm{d}\omega. \tag{13}$$

Using the definition of $\tilde{G}(s)$ in Eq. (10),

$$K_{\mathrm{opt}} = \frac{1}{2\omega_c}\int_{-\omega_c}^{\omega_c} \sum_{i=N+1}^{\infty} \frac{\left(\omega_i^2 - \omega^2\right)F_i}{\left(\omega_i^2 - \omega^2\right)^2 + 4\zeta_i^2\omega_i^2\omega^2} \mathrm{d}\omega. \tag{14}$$

The integral above needs to be solved in order to obtain the optimal feedthrough matrix for the pointwise model.

4. Problem statement for spatial (MIIO) models

Now, consider the spatial system in Eq. (2). This could represent the model associated with a flexible beam, relating the actuator signals to the transverse deflection at any point along the beam. A suitable feedthrough term is desired to compensate for the truncation error of the truncated model of the system. This feedthrough term, K_r, is added to the truncated model, G_{rN}. The corrected model is

$$\hat{G}_r(s, r) = G_{rN}(s, r) + K_r(r) \tag{15}$$

and K_r is chosen in the following form [6]:

$$K_r(r) = \sum_{i=N+1}^{\infty} \phi_i(r)K_{ri} \tag{16}$$

where $K_{ri} \in \mathbf{R}^{1\times n}$ and $\phi_i(r)$ is again the eigenfunction associated with mode i.

The spatial $\mathscr{H}_2$ norm of a spatial system, $U(s,r)$, is defined as [10,11],

$$\langle\!\langle U(s,r)\rangle\!\rangle_2^2 = \frac{1}{2\pi}\int_{-\infty}^{\infty}\int_{\mathscr{R}} \operatorname{trace}\{U^*(j\omega,r)U(j\omega,r)\}\,\mathrm{d}r\mathrm{d}\omega. \tag{17}$$

The spatial $\mathscr{H}_2$ norm of a system takes into account the spatial information embedded in the model. It can be regarded as a measure of the spatial output energy of a system which can be useful when dealing with spatially distributed systems.

Now, following the method in [6], K_{ri} is determined such that the spatial $\mathscr{H}_2$ norm of the weighted error between the full-order model (2) and the corrected model (15) is minimised. The cost function is defined as

$$\begin{aligned} J_r &= \big\langle\!\big\langle W_r(s,r)\big(G_r(s,r) - \hat{G}_r(s,r)\big)\big\rangle\!\big\rangle_2^2 \\ &= \big\langle\!\big\langle W_r(s,r)\big(\tilde{G}_r(s,r) - K_r(r)\big)\big\rangle\!\big\rangle_2^2 \end{aligned} \tag{18}$$

where

$$\tilde{G}_r(s,r) = \sum_{i=N+1}^{\infty} \frac{\phi_i(r)P_i}{s^2 + 2\zeta_i\omega_i s + \omega_i^2} \tag{19}$$

and $W_r(s,r)$ is a diagonal matrix whose elements are ideal low-pass filters distributed spatially over $\mathscr{R}$ [6],

$$W_r = \operatorname{diag}(w_r, w_r, \ldots, w_r) \tag{20}$$

where

$$w_r(j\omega,r) = \begin{cases} 1, & -\omega_c \leqslant \omega \leqslant \omega_c, r \in \mathscr{R}, \\ 0, & \text{otherwise} \end{cases} \tag{21}$$

and $\omega_c \in (\omega_N, \omega_{N+1})$ is the-cut-off frequency of each low-pass filter.

The cost function in Eq. (l8) can be shown to be

$$\begin{aligned} J_r &= \big\langle\!\big\langle W_r(s,r)\tilde{G}_r(s,r)\big\rangle\!\big\rangle_2^2 + \frac{1}{2\pi}\int_{-\omega_c}^{\omega_c} \operatorname{trace}\{K_r(r)^T K_r(r)\}\,\mathrm{d}r\,\mathrm{d}\omega \\ &\quad - 2\times\frac{1}{2\pi}\int_{-\omega_c}^{\omega_c}\int_{\mathscr{R}} \operatorname{Re}\{\operatorname{trace}\{\tilde{G}_r(j\omega,r) * K_r(r)\}\}\,\mathrm{d}r\,\mathrm{d}\omega \\ &= \big\langle\!\big\langle W_r(s,r)\tilde{G}_r(s,r)\big\rangle\!\big\rangle_2^2 \\ &\quad + \frac{1}{2\pi}\int_{-\omega_c}^{\omega_c}\int_{\mathscr{R}} \operatorname{trace}\left\{\left(\sum_{i=N+1}^{\infty}\phi_i(r)K_{ri}^T\right)\times\left(\sum_{l=N+1}^{\infty}\phi_l(r)K_{rl}\right)\right\}\mathrm{d}r\,\mathrm{d}\omega \\ &\quad - 2\times\frac{1}{2\pi}\int_{-\omega_c}^{\omega_c}\int_{\mathscr{R}} \operatorname{Re}\left\{\operatorname{trace}\left\{\left(\sum_{i=N+1}^{\infty}\frac{\phi_i(r)P_i^T}{(\omega_i^2-\omega^2) - 2\zeta_i\omega_i\omega j}\right)\right.\right. \\ &\quad \left.\left.\times\left(\sum_{l=N+1}^{\infty}\phi_l(r)K_{rl}\right)\right\}\right\}\mathrm{d}r\,\mathrm{d}\omega. \end{aligned} \tag{22}$$

Using the orthogonality property of the eigenfunction (3),

$$J_r = \left\langle\left\langle W_r(s,r)\tilde{G}_r(s,r)\right\rangle\right\rangle_2^2 + 2\omega_c \times \frac{1}{2\pi} \times \text{trace}\left\{\sum_{i=N+1}^{\infty} \Phi_i^2 K_{ri}^T K_{ri}\right\} - 2 \times \frac{1}{2\pi}\int_{-\omega_c}^{\omega_c} \text{Re}\left\{\text{trace}\left\{\sum_{i=N+1}^{\infty}\left(\frac{\Phi_i^2 P_i^T K_{ri}}{(\omega_i^2-\omega^2)-2\zeta_i\omega_i\omega j}\right)\right\}\right\} \mathrm{d}\omega \tag{23}$$

Differentiating J_r with respect to K_{ri} (see [14], p. 592) and setting this value to a zero vector for optimality,

$$\frac{\mathrm{d}J}{\mathrm{d}K_{ri}} = 2 \times 2\omega_c \times \frac{1}{2\pi}\Phi_i^2 K_{ri}^{\text{opt}} - 2 \times \frac{1}{2\pi}\int_{-\omega_c}^{\omega_c} \text{Re}\left\{\frac{\Phi_i^2 P_i}{(\omega_i^2-\omega^2)-2\zeta_i\omega_i\omega j}\right\} \mathrm{d}\omega = 0 \tag{24}$$

The optimal K_{ri} is

$$K_{ri}^{\text{opt}} = \frac{1}{2\omega_c}\int_{-\omega_c}^{\omega_c} \frac{(\omega_i^2-\omega^2)P_i}{(\omega_i^2-\omega^2)^2+4\zeta_i^2\omega_i^2\omega^2}\,\mathrm{d}\omega. \tag{25}$$

It is interesting that the optimal solution of the spatial case, K_{ri}^{opt}, in Eq. (25) involves the same integral as that of the pointwise case, K^{opt}, in Eq. (14). In the next section, an analytical solution for the integral will be presented.

5. Solutions to the model correction problems

The integral in Eqs. (14) and (25) can be evaluated as follows (see Appendix A for derivations):

$$L = \int_{-\omega_c}^{\omega_c} \frac{\omega_i^2-\omega^2}{(\omega_i^2-\omega^2)^2+4\zeta_i^2\omega_i^2\omega^2}\,\mathrm{d}\omega. = \frac{1}{2\omega_i\sqrt{1-\zeta_i^2}} \ln\left(\frac{\omega_c^2+2\omega_c\omega_i\sqrt{1-\zeta_i^2}+\omega_i^2}{\omega_c^2-2\omega_c\omega_i\sqrt{1-\zeta_i^2}+\omega_i^2}\right). \tag{26}$$

Having obtained the solution to the integral, the optimal feedthrough terms for the pointwise and spatial models can be observed.

5.1. Pointwise models, K_{opt}

From Eq. (26), the solution for K_{opt} for pointwise models (14) is

$$K_{\text{opt}} = \frac{1}{4\omega_c}\sum_{i=N+1}^{\infty} \frac{1}{\omega_i\sqrt{1-\zeta_i^2}} \ln\left(\frac{\omega_c^2+2\omega_c\omega_i\sqrt{1-\zeta_i^2}+\omega_i^2}{\omega_c^2-2\omega_c\omega_i\sqrt{1-\zeta_i^2}+\omega_i^2}\right) F_i. \tag{27}$$

It is interesting to compare Eq. (27) with the optimal solution for K_{opt} for the case when there is no damping. As reported in [7], if $\zeta_i = 0$, $\forall i$, then $K_{\text{opt}} = (1/2\omega_c)$

$\sum_{i=N+1}^{\infty}(1/\omega_i)\ln\big((\omega_i+\omega_c)/(\omega_i-\omega_c)\big)F_i$. It can be shown that

$$\ln\left(\frac{\omega_c^2+2\omega_c\omega_i\sqrt{1-\zeta_i^2}+\omega_i^2}{\omega_c^2-2\omega_c\omega_i\sqrt{1-\zeta_i^2}+\omega_i^2}\right)\to 2\ln\left(\frac{\omega_i+\omega_c}{\omega_i-\omega_c}\right)\quad\text{as}\quad\zeta_i\to 0.$$

Hence, as $\zeta_i\to 0$,

$$K_{\text{opt}}\to\frac{1}{2\omega_c}\sum_{i=N+1}^{\infty}\frac{1}{\omega_i}\ln\left(\frac{\omega_i+\omega_c}{\omega_i-\omega_c}\right)F_i. \tag{28}$$

Therefore, the optimal correction term determined here is consistent with the results previously reported in the literature.

5.2. Spatial models, K_{ri}^{opt}

The optimal feedthrough term for the spatial model can now be determined as in Eq. (16) with

$$K_{ri}^{\text{opt}}=\frac{1}{4\omega_c\omega_i\sqrt{1-\zeta_i^2}}\ln\left(\frac{\omega_c^2+2\omega_c\omega_i\sqrt{1-\zeta_i^2}+\omega_i^2}{\omega_c^2-2\omega_c\omega_i\sqrt{1-\zeta_i^2}+\omega_i^2}\right)P_i. \tag{29}$$

In [6], it is shown that the solution for $\zeta_i=0,\ \ \forall i$ is $K_{ri}^{\text{opt}}=\big(1/(2\omega_c\omega_i)\big)\ln\big((\omega_i+\omega_c)/(\omega_i-\omega_c)\big)P_i$. Comparing the above solution with that for the no damping case, it can be verified that as $\zeta_i\to 0$,

$$K_{ri}^{\text{opt}}\to\frac{1}{2\omega_c\omega_i}\ln\left(\frac{\omega_i+\omega_c}{\omega_i-\omega_c}\right)P_i. \tag{30}$$

Hence, the correction term for the spatial model presented above, approaches to the case with no damping [6].

The contribution of higher frequency modes to the feedthrough terms for pointwise and spatial systems decreases as i increases. Hence, in practice, it is sufficient to include a relatively large number of out-of-bandwidth modes to calculate these optimal feedthrough terms. The solution presented here can be used to find the optimal feedthrough term for more realistic resonant systems (pointwise and spatial systems) with non-zero damping.

The solutions for feedthrough terms that are proposed in [6,7] ignore the effect of damping. Those solutions are actually special cases of the solutions proposed in this paper when $\zeta_i=0,\ \ \forall i$ as explained in the previous section. Naturally, if the system includes damping, one would expect the correction terms derived above to result in a better corrected model.

For each mode i, the contribution to the feedthrough term in Eqs. (27) and (29) is proportional to k_i,

$$k_i=\frac{1}{\omega_i\sqrt{1-\zeta_i^2}}\ln\left(\frac{\omega_c^2+2\omega_c\omega_i\sqrt{1-\zeta_i^2}+\omega_i^2}{\omega_c^2-2\omega_c\omega_i\sqrt{1-\zeta_i^2}+\omega_i^2}\right). \tag{31}$$

If the resonance frequency is expressed as $\omega_i = k_{\omega i}\omega_c$, then k_i may be re-written as

$$k_i = \frac{1}{k_{\omega i}\omega_c\sqrt{1-\zeta_i^2}} \ln\left(\frac{1+2k_{\omega i}\sqrt{1-\zeta_i^2}+k_{\omega i}^2}{1-2k_{\omega i}\sqrt{1-\zeta_i^2}+k_{\omega i}^2}\right). \tag{32}$$

The normalised k_i is then obtained by dividing k_i (32) with the arbitrary reference k_i that is evaluated at $\zeta_i = 0, k_{\omega i} = 1.5$. The plot in Fig. 1 shows the change in the normalised k_i value as the damping ratio and the resonance frequency with respect to the cut-off frequency (ω_i/ω_c) are varied. At large (ω_i/ω_c) ratio, the effect of damping on the normalised k_i is minimal. There is small difference between the results with and without the damping effect. However, at smaller ω_i/ω_c ratio, the difference becomes more significant. It can be observed that when the resonance frequency is relatively close to the cut-off frequency, the feedthrough term would give an excessive value if the damping effect is ignored. This is expected as when ω_i is close to ω_c, the effect of damping of that mode on the in-bandwidth modes is considerable. In fact, if the damping effect is ignored, the normalised k_i would have an infinite value when the resonance frequency is equal to the cut-off frequency.

6. Simulation results

Now, consider an example of a simply supported flexible beam, i.e. a 60 cm long uniform aluminium beam of a rectangular cross-section (50 mm × 3 mm) in Fig. 2. A pair of piezoelectric ceramic elements is attached symmetrically to either side of the beam, 50 mm away from one end of the beam. The piezoceramic elements used are PIC151 patches. These patches are 25 mm wide, 70 mm long and 0.25 mm thick. Physical properties of the piezoelectric patches and dimensions of the beam are taken from [15,16].

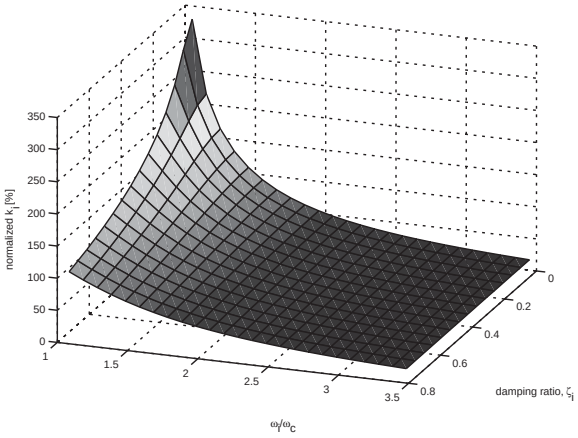

Fig. 1. Normalised k_i.

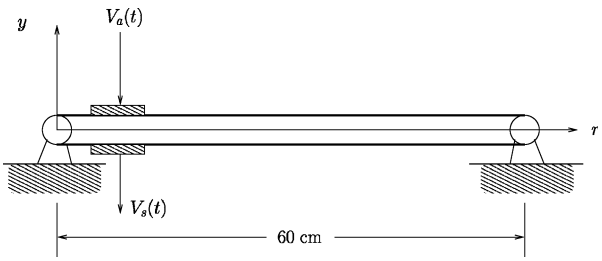

Fig. 2. A simply supported beam.

The governing partial differential equation of the beam is [1]

$$EI\frac{\partial^4 y(t,r)}{\partial r^4}+\rho A_b\frac{\partial^2 y(t,r)}{\partial t^2}=\frac{\partial^2 M_{pr}(t,r)}{\partial r^2} \tag{33}$$

where the beam transverse deflection at point r is y. The Young's modulus, moment of inertia, density and cross-sectional area of the beam are denoted by E, I, ρ and A_b, respectively. The right-hand side of Eq. (33) is the bending moment contribution by the piezoelectric actuator.

The model is obtained via modal analysis, where the damping factor associated with each mode, ζ_i, is added afterwards. Here, $\zeta_i = 0.025$ is used for each mode. The mode shapes ϕ_i are sinusoidal functions since the beam is pinned at both ends:

$$\phi_i(r)=\sqrt{\frac{2}{\rho A_b L}}\sin\left(\frac{i\pi r}{L}\right),\quad i=1,2,\ldots \tag{34}$$

where L is the length of the beam. The spatial model used is the transfer function from the piezoelectric actuator voltage to the transverse deflection y at point r along the beam. The model is similar to Eq. (2) with $P_i = \alpha\Psi_i$, where

$$\Psi_i=\frac{\mathrm{d}\phi_i(r_2)}{\mathrm{d}r}-\frac{\mathrm{d}\phi_i(r_1)}{\mathrm{d}r}. \tag{35}$$

Here, α is a constant that depends on the properties of the piezoelectric actuator patch and the beam. The locations of the ends of the patch are denoted by r_1 and r_2. Moreover, the pointwise model used is the transfer function from the piezoelectric actuator voltage, $V_a(t)$, to its collocated sensor voltage, $V_s(t)$.

The first 11 modes are used for the model, while higher frequency modes up to mode 100 are used for calculating the feedthrough terms. The cut-off frequency is chosen to be $\omega_c = 2682$ Hz, which is between modes 11 and 12. The simulation results are presented below.

6.1. Pointwise model

Fig. 3 compares the truncated and full-order models up to the frequency ω_c. It can be observed that there are errors in the locations of zeros and in the amount of d.c. content of the truncated model. Fig. 4 shows the effect of adding a feedthrough term to the truncated model, where the

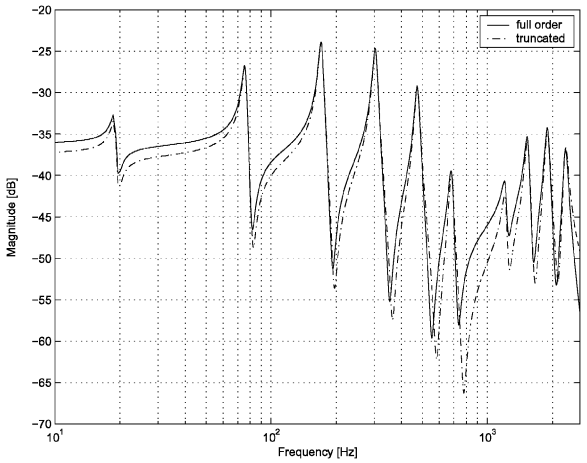

Fig. 3. Comparison of truncated and full-order models.

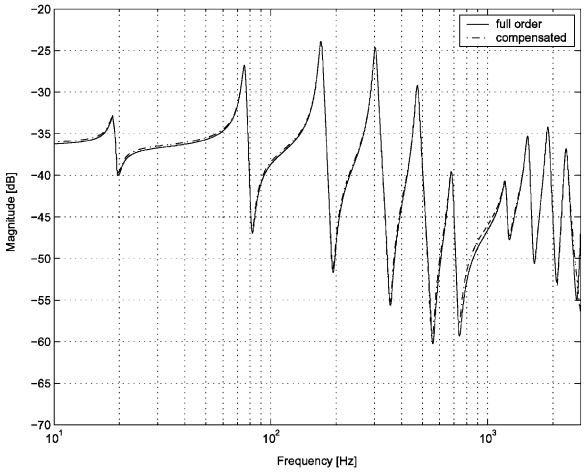

Fig. 4. Comparison of full-order and compensated models.

errors in the locations of zeros and in the d.c. content of the compensated model are reduced substantially.

The frequency responses (magnitude) of the error systems corresponding to both methods are presented in Fig. 5. The error system is based on the error associated with the corrected model with respect to the full-order model. The full-order model here consists of modes from 1 to 100. The first error system is based on the method that ignores the damping effect [7], while the second is based on the proposed method that incorporates the damping effect in the feedthrough term. The second method has a lower magnitude of error at low frequencies, while the first method has a slightly lower error at high frequencies. However, although the first method (that ignores damping) has a smaller error at some frequencies, the second method (that includes damping) has in fact a smaller weighted $\mathscr{H}_2$ norm of the error system. The result is obvious since the first

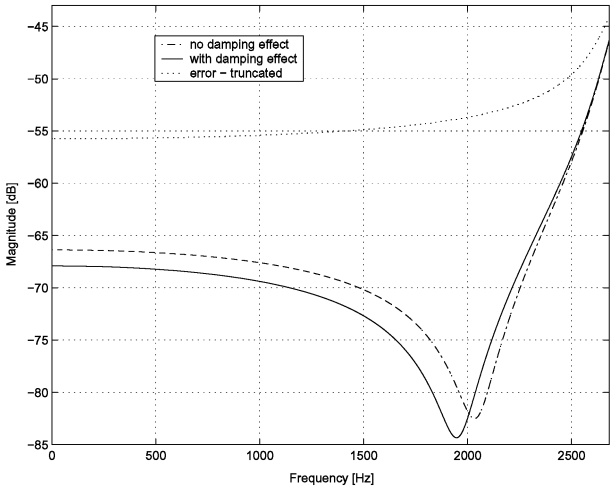

Fig. 5. Frequency responses of error systems.

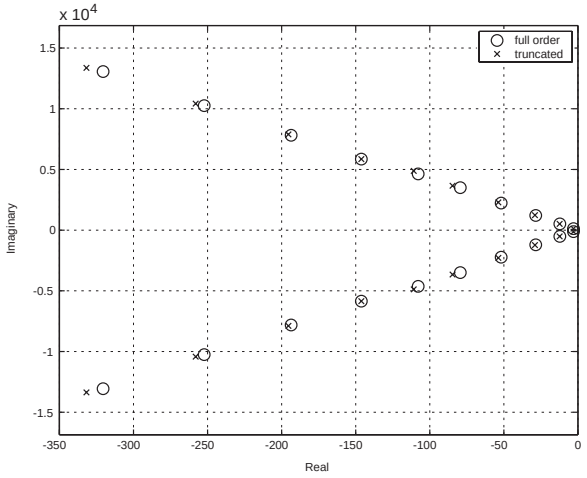

Fig. 6. Zeros of full-order and truncated models.

method is a special case of the second method and the cost function, i.e. the weighted $\mathscr{H}_2$ norm of the error system, is convex with respect to the feedthrough term. Hence, the minimum cost function is obtained via the compensation method with damping. It can also be seen from Fig. 5 that the performance of the second method is better for a wider range of frequencies of interest. The effect of damping would be more significant when the system is more heavily damped. Finally, when both error systems are compared to the error system associated with the truncated model as shown in Fig. 5, it is obvious that both methods produce significantly lower errors at all in-bandwidth frequencies.

Fig. 6 compares the zeros of the full-order and truncated models. There are errors in the locations of zeros due to the removal of out-of-bandwidth modes. The effect of adding a

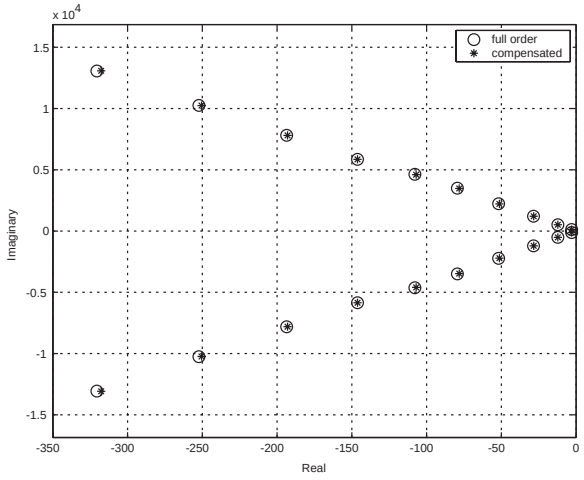

Fig. 7. Zeros of full-order and corrected models.

feedthrough term to the truncated model can be seen in Fig. 7. The locations of zeros are considerably improved once the feedthrough term is added to the truncated model.

Having observed the effect of compensation on the d.c. content and location of zeros of the truncated model, it would be interesting to see how the compensation affects controller design. Would there be any significant difference in controller performance for a controller that is based on a truncated model compared to a controller that is based on a compensated model? In order to answer the question, the following simulation is performed. A truncated model with only the first two in-bandwidth modes is chosen so the effect of controller on the first two modes can be easily observed. The cut-off frequency used is $\omega_c = 128\,\text{Hz}$, and modes 3–100 are used as out-of-bandwidth modes. In this demonstration, we use the $\mathscr{H}_\infty$ control design approach for developing the controllers although other control design methods can also be used instead.

Initially, a model obtained via direct truncation is used to design the optimal controller. The system used is

$$\begin{aligned} \dot{x}(t) &= Ax(t) + Bw(t) + Bu(t) \\ z(t) &= \begin{bmatrix} C \\ 0 \end{bmatrix} x(t) + \begin{bmatrix} 0 \\ 0 \end{bmatrix} w(t) + \begin{bmatrix} 0 \\ \varepsilon_1 \end{bmatrix} u(t) \\ y(t) &= Cx(t) + \varepsilon_2 w(t) \end{aligned} \tag{36}$$

where $(A, B, C, 0)$ is the state-space realisation of the truncated pointwise model of the piezoelectric beam described previously. The disturbance input, w, and the control input, u, enter through the same channel. The states are contained in x and the performance output is z, while the measured output is described by y. Here, ε_1 and ε_2 are incorporated to satisfy the full-rank requirement in Matlab optimisation using HINFOPT command. The controller obtained is based on $\varepsilon_1 = 1.1 \times 10^{-2}$ and $\varepsilon_2 = 1.0 \times 10^{-2}$ which optimises γ such that $\|\gamma T_{zw}\|_\infty \leqslant 1$ and T_{zw} is the closed-loop transfer function from w to z. Fig. 8 shows the expected closed-loop result based on the truncated model. It can be seen that the controller reduces the resonance response of the

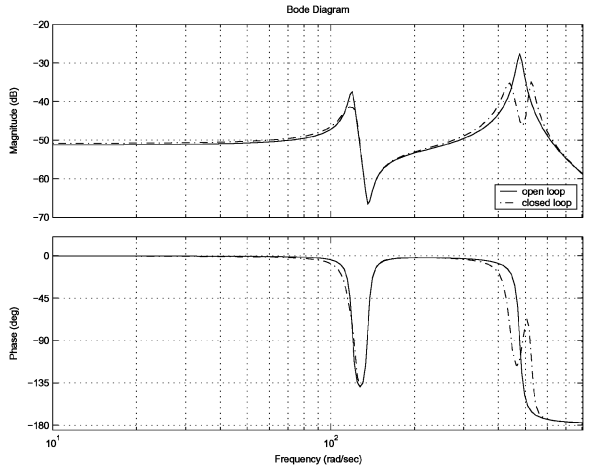

Fig. 8. Bode plot based on the truncated model.

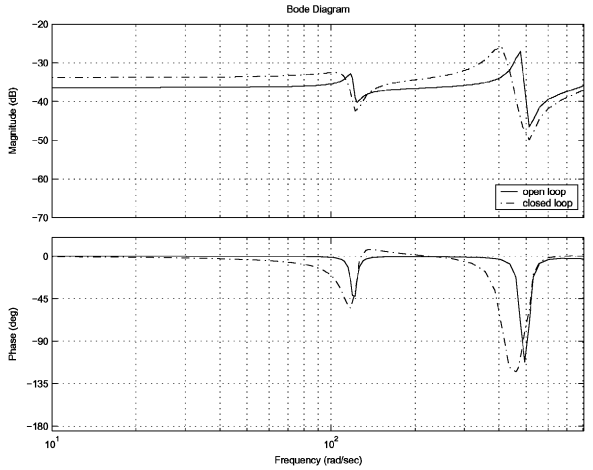

Fig. 9. Bode plot of the truncated-model-based controller applied to the full-order system.

second mode by about 17 dB. However, when the controller is implemented on the full-order model, the closed-loop result is significantly different. There is an increase in the response at most in-bandwidth frequencies as shown in Fig. 9. This may be expected because there are errors in the d.c. content and location of zeros in the truncated model due to truncation of high-frequency dynamics. Even though the system is stable with a gain margin of 11.5 dB and a phase margin of -25.1° when analysed with the full-order model, the closed-loop performance has degraded significantly. The results show a considerable uncertainty that the designed controller would not perform as expected because the truncated model does not sufficiently reflect the in-bandwidth dynamics of the full-order model.

Next, it is interesting to see whether model compensation would actually help in improving the performance of the controller. For this purpose, an optimal $\mathscr{H}_\infty$ controller is designed based on

the compensated model

$$\begin{aligned}\dot{x}(t) &= Ax(t) + Bw(t) + Bu(t)\\ z(t) &= \begin{bmatrix} C \\ 0 \end{bmatrix} x(t) + \begin{bmatrix} D \\ 0 \end{bmatrix} w(t) + \begin{bmatrix} D \\ \varepsilon \end{bmatrix} u(t)\\ y(t) &= Cx(t) + Dw(t) + Du(t)\end{aligned} \tag{37}$$

where (A, B, C, D) is the state-space realisation of the compensated pointwise model, where D is the compensation feedthrough term. Other parameters have been described previously. The optimal controller is computed based on $\varepsilon = 1.6 \times 10^{-2}$ and Fig. 10 shows the expected

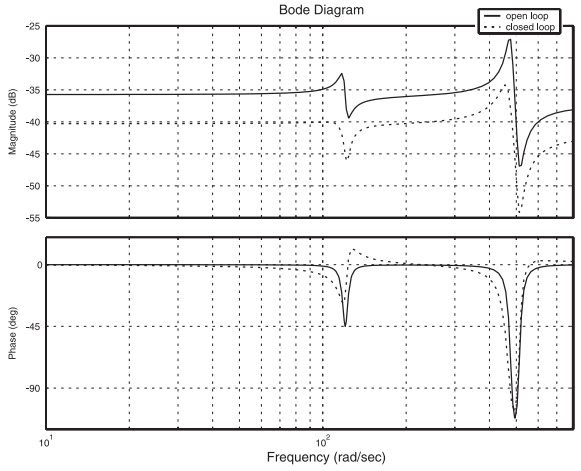

Fig. 10. Bode plot based on the corrected model.

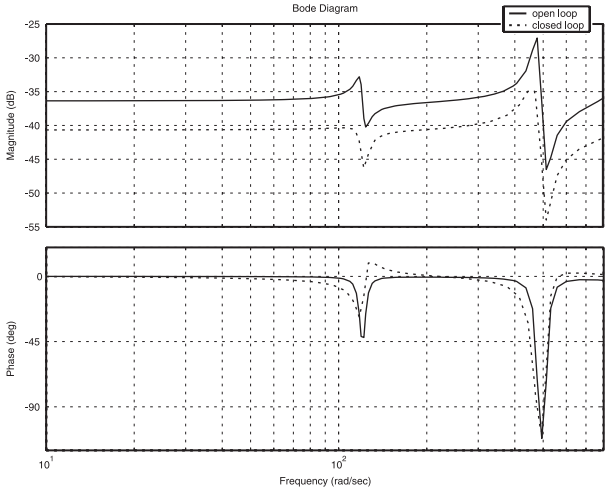

Fig. 11. Bode plot of the corrected-model-based controller applied to the full-order system.

closed-loop result. Comparing Fig. 11 with Fig. 10 shows that the obtained control performs as expected when it is applied to the full-order system. The system has a theoretical infinite gain margin and a phase margin of 34.6° when analysed using the full-order model. Therefore, it is clear that a more accurate controller design can be obtained by compensating the truncated model. By compensating the truncated model, the dimensions of the low-order model stays the same; however, the accuracy of the model can be significantly enhanced.

6.2. Spatial model

The performance of the proposed method in compensating for the truncation error of a spatial system can be seen from Figs. 12–15. The figures show the frequency responses (magnitude) of

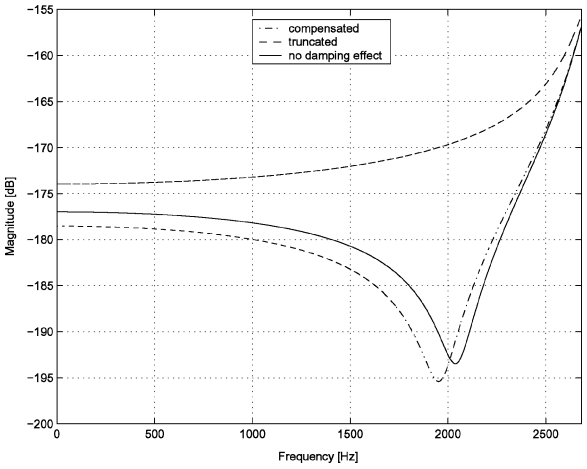

Fig. 12. Frequency responses of error systems at $r = 0.13$ m.

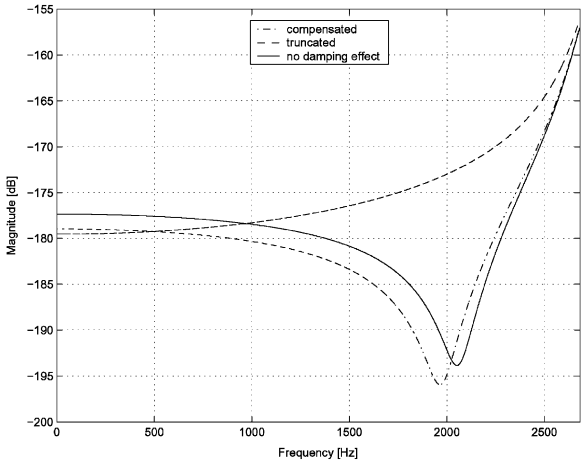

Fig. 13. Frequency responses of error systems at $r = 0.27$ m.

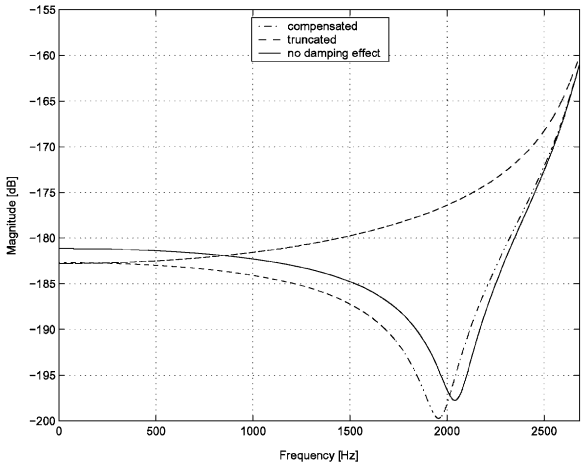

Fig. 14. Frequency responses of error systems at $r = 0.36$ m.

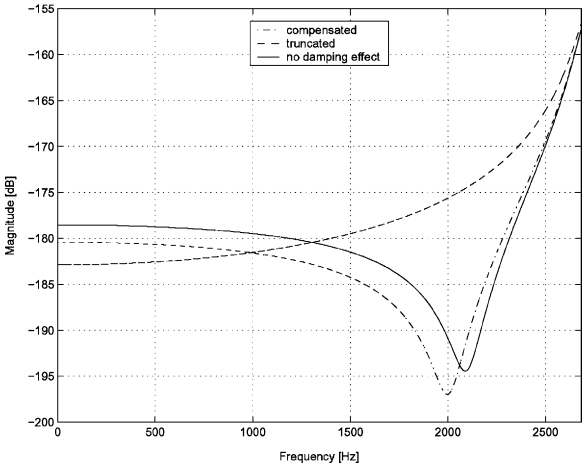

Fig. 15. Frequency responses of error systems at $r = 0.47$ m.

error responses at four different locations along the beam at $r = 0.13, 0.27, 0.36$ and 0.47 m. The magnitudes of error systems for truncated models, and corrected models with and without the damping effect are shown in the plots. Similar to the case of pointwise models, the compensation method with the damping effect in general performs better (i.e. it produces a smaller weighted spatial $\mathscr{H}_2$ norm of the error system) than the non-damping compensation method proposed in [6]. This can be explained in a similar way as in the case of the pointwise model. The optimisation cost function is the weighted spatial $\mathscr{H}_2$ norm of the error system which is shown to be convex with respect to the feedthrough term. Since the non-damping case is a special case of the damping case, the compensation method with damping will have to yield a smaller cost compared to the non-damping compensation method. The fact that the feedthrough term is obtained from the minimisation of the weighted spatial $\mathscr{H}_2$ norm of the error system implies that the feedthrough term minimises the error in a spatially averaged sense across the beam. Thus, when compared to

the error of the truncated model, a slightly larger error may result at some locations on the structure over a certain frequency range (e.g. at $r = 0.27, 0.47\,m$), but the overall spatial error of the corrected model will be minimum. In some resonant systems that are more heavily damped such as acoustic systems [17], the advantage of the proposed method over the previous method would be more pronounced.

Next, a truncated model with only the first two in-bandwidth modes is considered, with the purpose of showing the effect of the feedthrough term more clearly. The cut-off frequency used is $\omega_c = 128$ Hz, while the highest out-of-bandwidth mode considered for the feedthrough term is mode 100. Figs. 16 and 17 show the spatial error frequency responses for the truncated and corrected models, respectively. The error corresponding to the truncated model increases with frequency, while the error associated with the corrected model decreases to a minimum at the mid-frequency region. From the plots, the error of the truncated model ranges from -180 to -136 dB spatially, while the error of the corrected model ranges from -210 to -146 dB spatially. It is obvious that the corrected model produces a lower error over the entire structure.

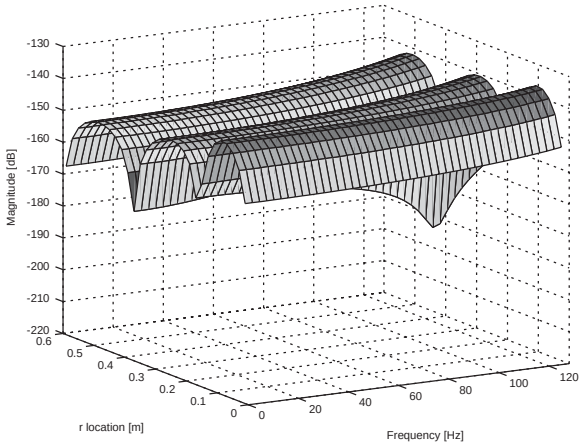

Fig. 16. Spatial error frequency response for the truncated model.

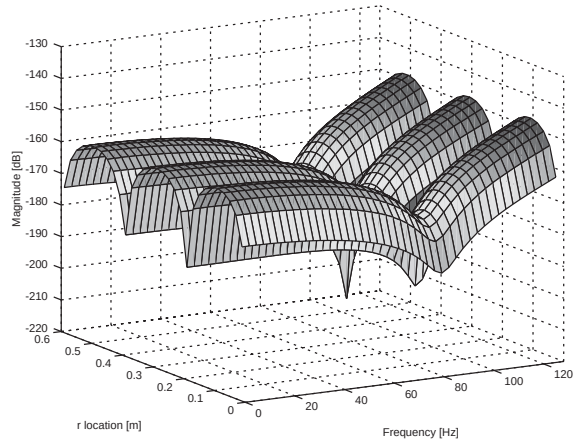

Fig. 17. Spatial error frequency response for the corrected model.

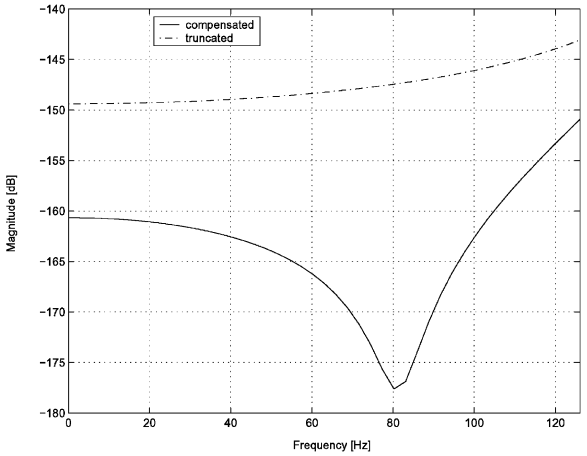

Fig. 18. Spatially averaged error frequency responses.

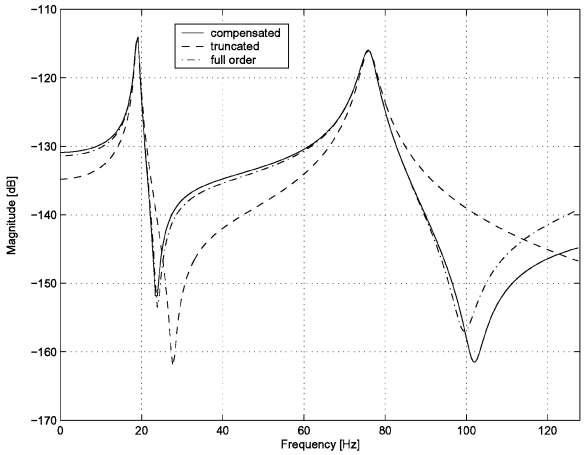

Fig. 19. Comparison of pointwise frequency responses at $r = 0.10\,\mathrm{m}$.

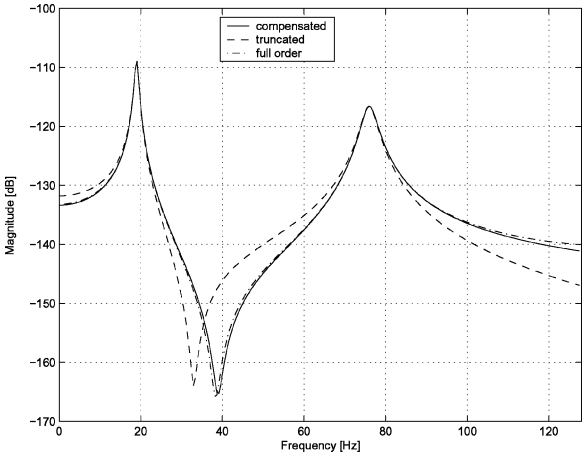

Fig. 20. Comparison of pointwise frequency responses at $r = 0.21\,\mathrm{m}$.

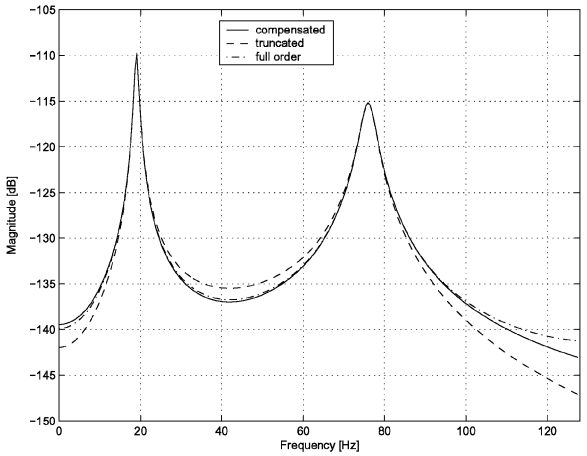

Fig. 21. Comparison of pointwise frequency responses at $r = 0.42$ m.

Fig. 18 compares the spatially averaged error frequency responses for the truncated and compensated models. It is obvious that the compensated model performs better spatially than the truncated model.

Figs. 19–21 show the comparison of pointwise frequency responses at several locations along the beam where $r = 0.10, 0.21$ and 0.42 m. It can be observed that the compensated frequency responses significantly reduce the errors in the zero locations and the gains when compared to the truncated frequency responses. The simulation results show the effectiveness of the proposed method in compensating for the truncation error spatially.

7. Conclusions

Analytical solutions for compensating for the truncation error in the pointwise and spatial models of resonant systems have been presented. It is shown that adding a feedthrough term to the truncated model improves the zero locations and d.c. content of the model as confirmed by the simulations. The contribution of damping in the models of resonant systems is considered, where the damping effect is shown to be important especially when the modes are heavily damped. It is observed that the proposed solutions are consistent with the previous solutions that ignore the effect of damping. There is no limitation on the number of out-of-bandwidth modes that can be used in evaluating the feedthrough terms, since the terms can be readily computated from the analytical solutions. Therefore, the proposed solution provides an efficient way to obtain lower-order pointwise and spatial models of resonant systems that include damping.

Appendix A. The integral solution

Here, the integral that is required for the expressions in Eqs. (14) and (25) is solved analytically. The authors were not able to locate a full analytical solution for the integral in standard references

[18–20]. The integral can be divided into two parts:

$$L = \int_{-\omega_c}^{\omega_c} \frac{\omega_i^2 - \omega^2}{\left(\omega_i^2 - \omega^2\right)^2 + 4\zeta_i^2\omega_i^2\omega^2}\,\mathrm{d}\omega$$
$$= \omega_i^2 L_1 - L_2. \tag{A.1}$$

where

$$L_1 = 2\int_0^{\omega_c} \frac{1}{(\omega_i^2 - \omega^2)^2 + 4\zeta_i^2\omega_i^2\omega^2}\,\mathrm{d}\omega$$
$$L_2 = 2\int_0^{\omega_c} \frac{\omega^2}{(\omega_i^2 - \omega^2)^2 + 4\zeta_i^2\omega_i^2\omega^2}\,\mathrm{d}\omega. \tag{A.2}$$

Since both integrands are even functions of ω, it is sufficient to integrate them only from 0 to ω_c as in Eq. (A.2).

The denominator can be written as

$$(\omega_i^2 - \omega^2)^2 + 4\zeta_i^2\omega_i^2\omega^2 = \omega^4 + 2\omega_i^2\left(2\zeta_i^2 - 1\right)\omega^2 + \omega_i^4$$
$$= \left(\omega^2 - \omega_{r1}^2\right)\left(\omega^2 - \omega_{r2}^2\right) \tag{A.3}$$

where

$$\omega_{r1}^2 = \omega_i^2\left(\left(1 - 2\zeta_i^2\right) - 2\zeta_i\sqrt{1 - \zeta_i^2}j\right)$$
$$\omega_{r2}^2 = \omega_i^2\left(\left(1 - 2\zeta_i^2\right) + 2\zeta_i\sqrt{1 - \zeta_i^2}j\right) \tag{A.4}$$

and j is $\sqrt{-1}$. Here, only the underdamped case ($\zeta_i < 1$) is considered since the case captures the majority of resonant systems of interest. However, the solution for critically damped and overdamped cases can also be obtained in a more straightforward manner since ω_{r1}^2 and ω_{r2}^2 will be real numbers.

A.1. The first integral, L_1

The integrand of L_1 can be written as partial fractions:

$$\frac{1}{\left(\omega_i^2 - \omega^2\right)^2 + 4\zeta_i^2\omega_i^2\omega^2} = \frac{1}{\Omega_r}\left(\frac{1}{\left(\omega^2 - \omega_{r1}^2\right)} - \frac{1}{\left(\omega^2 - \omega_{r2}^2\right)}\right) \tag{A.5}$$

where

$$\Omega_r = \omega_{r1}^2 - \omega_{r2}^2$$
$$= -4\zeta_i\sqrt{1 - \zeta_i^2}\omega_i^2 j. \tag{A.6}$$

Consider the following indefinite integral with a complex constant, a. The solution to the indefinite integral is [21]

$$\int \frac{\mathrm{d}z}{z^2 - a^2} = \frac{1}{2a} \ln\left(\frac{z-a}{z+a}\right) + c \tag{A.7}$$

where c is a constant. The integral L_1 (A.2) can be solved by incorporating Eqs. (A.5) and (A.7) to give

$$L_1 = L_1^{\omega_c} - L_1^0 \tag{A.8}$$

where

$$L_1^{\omega} = \frac{1}{\Omega_r}\left\{\frac{1}{\omega_{r1}} \ln\left(\frac{\omega - \omega_{r1}}{\omega + \omega_{r1}}\right) - \frac{1}{\omega_{r2}} \ln\left(\frac{\omega - \omega_{r2}}{\omega + \omega_{r1}}\right)\right\}. \tag{A.9}$$

Define

$$\cos\,\alpha = 1 - 2\zeta_i^2. \tag{A.10}$$

Consequently,

$$\sin\,\alpha = 2\zeta_i\sqrt{1-\zeta_i^2}. \tag{A.11}$$

From Eqs. (A.10) and (A.11), the expressions in (A.4) and (A.6) can be re-written as

$$\begin{aligned} \omega_{r1} &= \omega_i \mathrm{e}^{\,-j\frac{\alpha}{2}} \\ \omega_{r2} &= \omega_i \mathrm{e}^{\,j\frac{\alpha}{2}} \\ \Omega_r &= -2\,\sin\,\alpha\omega_i^2 j. \end{aligned} \tag{A.12}$$

The following expressions can also be obtained:

$$\begin{aligned} \omega - \omega_{r1} &= r_a \mathrm{e}^{\,j\theta_a} \\ \omega + \omega_{r1} &= r_b \mathrm{e}^{\,-j\theta_b} \\ \omega - \omega_{r2} &= r_a \mathrm{e}^{\,-j\theta_a} \\ \omega + \omega_{r2} &= r_b \mathrm{e}^{\,j\theta_b} \end{aligned} \tag{A.13}$$

where

$$\begin{aligned} r_a &= \sqrt{\omega^2 - 2\omega\omega_i\,\cos(\alpha/2) + \omega_i^2} \\ r_b &= \sqrt{\omega^2 + 2\omega\omega_i\,\cos(\alpha/2) + \omega_i^2} \\ \theta_a &= \cot^{-1}\left(\frac{\omega - \omega_i\cos(\alpha/2)}{\omega_i\sin(\alpha/2)}\right) \\ \theta_b &= \cot^{-1}\left(\frac{\omega + \omega_i\cos(\alpha/2)}{\omega_i\sin(\alpha/2)}\right) \end{aligned} \tag{A.14}$$

and $\cot^{-1}(\Gamma)$ denotes the inverse cotangent of Γ.

From Eq. (A.13) the following expressions are obtained:

$$\ln\left(\frac{\omega-\omega_{r1}}{\omega+\omega_{r1}}\right)=\ln\left(\frac{r_a}{r_b}\right)+j(\theta_a+\theta_b)$$
$$\ln\left(\frac{\omega-\omega_{r2}}{\omega+\omega_{r2}}\right)=\ln\left(\frac{r_a}{r_b}\right)-j(\theta_a+\theta_b). \tag{A.15}$$

After some algebraic manipulation, it can be shown that L_1^{ω} (A.9) is real valued:

$$L_1^{\omega^3}=\frac{-1}{\omega\sin\alpha}\left\{\sin\frac{\alpha}{2}\ln\left(\frac{r_a}{r_b}\right)+\cos\frac{\alpha}{2}(\theta_a+\theta_b)\right\}. \tag{A.16}$$

Here, $\theta_a+\theta_b$, can be found from trigonometric identities [18],

$$\cot(\theta_a+\theta_b)=\frac{\cot\theta_a\cot\theta_b-1}{\cot\theta_a+\cot\theta_b}$$
$$=\frac{\omega^2-\omega_i^2}{2\omega\omega_i\sin(\alpha/2)}. \tag{A.17}$$

Realising that $\ln(r_a/r_b)$ can be written as $-0.5\ln(r_b^2/r_a^2)$ and using Eq. (A.17), the indefinite integral in Eq. (A.16) becomes

$$L_1^{\omega}=\frac{1}{2\omega_i^3\sin\alpha}\left\{\sin\frac{\alpha}{2}\ln\left(\frac{r_b^2}{r_a^2}\right)-2\cos\frac{\alpha}{2}\cot^{-1}\left(\frac{\omega^2-\omega_i^2}{2\omega\omega_i\sin(\alpha/2)}\right)\right\}. \tag{A.18}$$

Now, L_1 (A.8) can be evaluated from Eq. (A.18) by substituting ω with ω_c and 0, respectively:

$$L_1=\frac{1}{2\omega_i^3\sin\alpha}\left\{\sin\frac{\alpha}{2}\ln\left(\frac{\omega_c^2+2\omega_c\omega_i\cos(\alpha/2)+\omega_i^2}{\omega_c^2-2\omega_c\omega_i\cos(\alpha/2)+\omega_i^2}\right)\right.$$
$$\left.-2\cos\frac{\alpha}{2}\cot^{-1}\left(\frac{\omega_c^2-\omega_i^2}{2\omega_c\omega_i\sin(\alpha/2)}\right)+2\pi\cos\frac{\alpha}{2}\right\}. \tag{A.19}$$

By considering the trigonometric identities $\cos\alpha=2\cos^2(\alpha/2)-1=1-2\sin^2(\alpha/2)$ [19] and (A.10),

$$\cos\frac{\alpha}{2}=\sqrt{1-\zeta_i^2}$$
$$\sin\frac{\alpha}{2}=\zeta_i. \tag{A.20}$$

A.2. The second integral, L_2

Consider the second integral L_2 (A.2). The integrand can again be written as partial fractions:

$$\frac{\omega^2}{(\omega_i^2-\omega^2)^2+4\zeta_i^2\omega_i^2\omega^2}=\frac{1}{\Omega_r}\left(\frac{\omega_{r1}^2}{\omega^2-\omega_{r1}^2}-\frac{\omega_{r2}^2}{\omega^2-\omega_{r2}^2}\right). \tag{A.21}$$

Using Eq. (A.7), the integral becomes

$$L_2 = L_2^{\omega_c} - L_2^0 \tag{A.22}$$

where

$$L_2^{\omega} = \frac{1}{\Omega_r}\left\{\omega_{r1} \ln\left(\frac{\omega-\omega_{r1}}{\omega+\omega_{r1}}\right) - \omega_2 \ln\left(\frac{\omega-\omega_{r2}}{\omega+\omega_{r2}}\right)\right\}. \tag{A.23}$$

L_2^{ω} (A.23) can be shown, after some algebraic simplification, to be real valued as expected:

$$\begin{aligned} L_2^{\omega} &= \frac{-1}{\omega_i \sin\alpha}\left\{-\sin\frac{\alpha}{2}\ln\left(\frac{r_a}{r_b}\right) + \cos\frac{\alpha}{2}(\theta_a+\theta_b)\right\} \\ &= \frac{1}{2\omega_i \sin\alpha}\left\{-\sin\frac{\alpha}{2}\ln\left(\frac{r_b^2}{r_a^2}\right) - 2\cos\frac{\alpha}{2}\cot^{-1}\left(\frac{\omega^2-\omega_i^2}{2\omega\omega_i \sin(\alpha/2)}\right)\right\}. \end{aligned} \tag{A.24}$$

Then Eq. (A.22) can be evaluated using Eq. (A.24) after substitution of ω with ω_c and 0, respectively:

$$\begin{aligned} L_2 = \frac{1}{2\omega_i \sin\alpha}&\left\{-\sin\frac{\alpha}{2}\ln\left(\frac{\omega^2+2\omega_c\omega_i\cos(\alpha/2)+\omega_i^2}{\omega_c^2-2\omega_c\omega_i\cos(\alpha/2)+\omega_i^2}\right)\right\} \\ &- 2\cos\frac{\alpha}{2}\cot^{-1}\left(\frac{\omega_c^2-\omega_i^2}{2\omega_c\omega_i \sin(\alpha/2)}\right) + 2\pi\cos\frac{\alpha}{2} \end{aligned} \tag{A.25}$$

A.3. The integral solution, L

The original integral L (A.1) now can be solved from the solutions of the first (A.19) and second (A.25) integrals:

$$\begin{aligned} L &= \frac{1}{\omega_i \sin\alpha}\sin\frac{\alpha}{2}\ln\left(\frac{\omega^2+2\omega_c\omega_i\cos(\alpha/2)+\omega_i^2}{\omega_c^2-2\omega_c\omega_i\cos(\alpha/2)+\omega_i^2}\right) \\ &= \frac{1}{2\omega_i\cos(\alpha/2)}\ln\left(\frac{\omega_c^2+2\omega_c\omega_i\cos(\alpha/2)+\omega_i^2}{\omega_c^2-2\omega_c\omega_i\cos(\alpha/2)+\omega_i^2}\right) \end{aligned} \tag{A.26}$$

where $\cos(\alpha/2) = \sqrt{1-\zeta_i^2}$ (A.20).

References

[1] L. Meirovitch, Elements of Vibration Analysis, McGraw-Hill, New York, 1975.
[2] C.W. de Silva, Vibration: Fundamentals and Practice, CRC Press, Boca Raton, 2000.
[3] M. Green, D.J.N. Limebeer, Linear Robust Control, Prentice-Hall, Englewoods Cliffs, NJ, 1995.

[4] S.O.R. Moheimani, H.R. Pota, I.R. Petersen, Spatial balanced model reduction for flexible structures, Automatica 35 (1999) 269–277.
[5] R.L. Clark, Accounting for out-of-bandwidth modes in the assumed modes approach: implications on colocated output feedback control, Transactions of the ASME, Journal of Dynamic Systems, Measurement, and Control 119 (1997) 390–395.
[6] S.O.R. Moheimani, Minimizing the effect of out-of-bandwidth dynamics in the models of reverberant systems that arise in modal analysis: implications on spatial $\mathscr{H}_\infty$ control, Automatica 36 (2000) 1023–1031.
[7] S.O.R. Moheimani, Minimizing the effect of out of bandwidth modes in truncated structure models, ASME Journal of Dynamic Systems, Measurement, and Control 122 (2000) 237–239.
[8] S.O.R. Moheimani, W.P. Heath, Model correction for a class of spatio-temporal systems, in: Proceedings of the American Control Conference, Chicago, IL, USA, June 2000, pp. 3768–3772.
[9] R.L. Bisplinghoff, H. Ashley, Principles of Aeroelasticity, Dover, New York, 1975.
[10] S.O.R. Moheimani, M. Fu, Spatial $\mathscr{H}_2$ norm of flexible structures and its application in model order selection, in: Proceedings of the 37th IEEE Conference on Decision & Control, Tampa, FL, USA, December 1998, pp. 3623–3624.
[11] S.O.R. Moheimani, T. Ryall, Considerations in placement of piezoceramic actuators that are used in structural vibration control, in: Proceedings of the 38th IEEE Conference on Decision & Control, Phoenix, AZ, USA, December 1999, pp. 1118–1123.
[12] S.O.R. Moheimani, D. Halim, A convex optimization approach to the mode acceleration problem, in: Proceedings of the 15th IFAC World Congress, Barcelona, Spain, 2002.
[13] J.M.M. Silva, N.M.M. Maia, Modal Analysis and Testing, Kluwer Academic Publishers, Dordrecht, 1999.
[14] F.L. Lewis, Applied Optimal Control & Estimation: Digital Design & Implementation, Prentice-Hall, Englewood Cliffs, NJ, 1992.
[15] D. Halim, S.O.R. Moheimani, Spatial resonant control of flexible structures—application to a piezoelectric laminate beam, IEEE Transactions on Control Systems Technology.
[16] D. Halim, S.O.R. Moheimani, Spatial $\mathscr{H}_2$ control of a piezoelectric laminate beam: experimental implementation, IEEE Transactions on Control Systems Technology 10 (4) (2002) 533–546.
[17] T. Mckelvey, A.J. Fleming, S.O.R. Moheimani, Subspace-based system identification for an acoustic enclosure Transactions of the ASME, Journal of Vibration & Acoustics 124 (3) (2002) 414–419.
[18] D. Zwillinger (Ed.), CRC Standard Mathematical Tables and Formulae, 30th Edition, CRC Press, Boca Raton, Florida, 1996.
[19] R.S. Burington, Handbook of Mathematical Tables and Formulas, 5th Edition, McGraw-Hill, New York, 1973.
[20] A. Jeffrey (Ed.), Table of integrals, series, and products by I.S. Gradshteyn and I.M. Ryzhik, Academic Press, London, 1994.
[21] M.R. Spiegel, Schaum's Outline of Theory and Problems of Complex Variables: With an Introduction to Conformal Mapping and its Application, McGraw-Hill, Singapore, 1981.